Research Square

Preprints are preliminary reports that have not undergone peer review.
They should not be considered conclusive, used to inform clinical practice,
or referenced by the media as validated information.

An Exponential Scaling Kinetic Framework for High-Temperature Oxidation of Chromium and FeCrAl Alloys: Integrating Scale Volatilization and Reactive Element Sublayers

Irakli Nakhutsrishvili

iraklinakhutsrishvili52@gmail.com

Georgian Technical University https://orcid.org/0000-0002-7961-3437

Short Report

Keywords: High-temperature oxidation, Tedmon model, reactive element effect, scale volatilization, Lanthanum sublayer, Cerium buffering, transcendental kinetics

Posted Date: October 28th, 2026

DOI: https://doi.org/10.21203/rs.3.rs-11515761/v1

License: This work is licensed under a Creative Commons Attribution 4.0 International License.
Read Full License

Additional Declarations: The authors declare no competing interests.

An Exponential Scaling Kinetic Framework for High-Temperature Oxidation of Chromium and FeCrAl Alloys: Integrating Scale Volatilization and Reactive Element Sublayers (short communication)

I. Nakhutsrishvili
Georgian Technical University, 77 Kostava St., 0171 Tbilisi, Georgia
Contact E-mail: iraklinakhutsrishvili52@gmail.com
Submission ID a853d964-9576-4d46-b6ab-c1b5d465ac27

Abstract

The long-term thermodynamic stability of high-temperature alloys depends on the competitive equilibrium between parabolic oxide scale growth and linear mass loss via chemical volatilization. While the classical Tedmon equation provides a foundational baseline for these simultaneous processes, it assumes an invariant reaction surface and constant diffusion pathways over time. To transcend these limitations, this work introduces a generalized non-linear kinetic scaling framework incorporating an exponential dampening operator that directly maps the physical contraction of diffusion channels driven by reactive element sublayers. The predictive capability and universality of the proposed transcendental framework are systematically validated using two contrasting independent experimental configurations at 1100°C: a FeCrAl(La) alloy oxidized in ambient air and an unalloyed Cr+0.5Ce matrix evaluated under a reduced oxygen partial pressure (P_{O_2}=0.01 atm). For the FeCrAl(La) alloy, the derived numerical scaling achieves perfect convergence with empirical thermogravimetric curves, mathematically isolating a regime of absolute diffusion arrest ($dm/dt \to 0$) at a terminal mass gain of $m \cong 0.283$ mg·cm^{-2}, which aligns with the formation of a dense, continuous Lanthanum-rich interfacial sublayer observed via scanning electron microscopy (SEM). Conversely, under reduced oxygen potentials, a comparative residual analysis demonstrates a transition threshold where open-surface scale volatilization outpaces rigid sublayer establishment, shifting the kinetics toward the Tedmon boundary. By integrating explicit microstructural evidence with complex transcendental solutions, the developed framework establishes a mathematically rigorous diagnostic tool capable of predicting phase boundary transition thresholds under varying ambient oxygen potentials.

Keywords: High-temperature oxidation, Tedmon model, reactive element effect, scale volatilization, Lanthanum sublayer, Cerium buffering, transcendental kinetics.

High-temperature materials deployed in aggressive environments rely heavily on the continuous establishment of a slow-growing, highly adherent protective oxide scale, typically chromia (Cr_2O_3) or alumina (Al_2O_3). However, at elevated thermal boundaries, the long-term integrity of these scales is systematically threatened by two degrading phenomena: scale spallation driven by thermal expansion mismatches and chemical volatilization. The latter mechanism is particularly critical for chromia-forming and high-temperature chromia-containing alloy systems, where solid Cr_2O_3 undergoes further oxidation to highly volatile gaseous species (chiefly CrO_3, resulting in a continuous loss of material mass and accelerated degradation kinetics. The simultaneous processes of parabolic oxide growth and linear volatilization loss were historically formalized by Tedmon, providing a foundational mathematical baseline by assuming a constant volatilization rate and a steady-state scale thickness where growth and consumption rates reach equilibrium. Despite its widespread legacy application, the conventional Tedmon model operates under oversimplified boundary

conditions, assuming that the diffusion paths and reaction surface area remain invariant over the entire duration of exposure. In real alloy systems, especially those modified by reactive elements (REs) such as Cerium (Ce) or Lanthanum (La), the microstructural evolution at the scale/alloy interface diverges fundamentally from these idealized assumptions [1–4].

The integration of rare-earth reactive elements – a phenomenon widely known as the Reactive Element Effect (REE) – dramatically modifies the high-temperature oxidation mechanism. Microstructural and spectroscopic evidence confirms that reactive elements tend to segregate along oxide grain boundaries and form a dense, protective sublayer at the phase boundary. This sublayer acts as a powerful diffusion barrier that effectively blocks the outward migration of metal cations, forcing the scale to grow almost exclusively via the inward transport of oxygen anions. Consequently, the available reaction surface and effective diffusion area shrink non-linearly over time, rendering the classical parabolic rate constant highly time-dependent [5–8]. To transcend the limitations of the Tedmon paradigm, this work introduces a generalized, non-linear kinetic framework incorporating a modified differential scaling approach. By introducing an exponential dampening term into the growth function, our model directly maps the physical attenuation of diffusion channels driven by reactive element sublayers. To validate the predictive capability and universality of this mathematical model, we evaluate it against independent experimental datasets for Cerium-doped chromium under reduced oxygen pressures, alongside newly derived experimental kinetics for FeCrAl(La) alloys under intense thermal boundaries at 1100°C.
To overcome the microstructural limitations of the classical Tedmon paradigm, the net rate of mass change (dm/dt) during high-temperature oxidation is dictated by the dynamic competition between the protective scale growth controlled by reactive element segregation and the continuous mass loss driven by volatilization. Under these combined boundary conditions, the physical system can be mathematically formalized through two alternative non-linear differential pathways [2]:

$$\frac{\mathrm{dm}}{\mathrm{dt}} = \mathrm{k_r e^{-km}} - \mathrm{v_g}, \tag{1}$$

$$\frac{\mathrm{dm}}{\mathrm{dt}} = \frac{\mathrm{k_p}}{\mathrm{2m}} \mathrm{e^{-km}} - \mathrm{v_g}, \tag{2}$$

where m is the specific mass gain ($mg \cdot cm^{-2}$) isolated from the volatilization component, k_r and k_p are the rectilinear and parabolic oxidation rate constants, v_g represents the linear volatilization rate of the gaseous scale phase, and k is the exponential dampening coefficient. The exponential term (e^{-km}) serves as a functional operator mapping the physical contraction of diffusion pathways driven by the continuous thickening and densification of the reactive element sublayer. The fundamental mathematical complexity arises when attempting to solve the non-linear differential equation (2) to obtain an explicit analytical expression for time as a function of mass. Separating the variables in equation (2) yields the following transcendental integral:

$$\mathrm{t} = \int_0^{\mathrm{m}} \frac{2\mathrm{m e^{km}}}{\mathrm{k_p - 2m v_g e^{km}}} \mathrm{dm}. \tag{3}$$

Due to the presence of the linear mass variable directly modulating the exponential function in the denominator, integral (3) belongs to a class of non-linear transcendental functions that cannot be expressed in terms of elementary functions. This mathematical profile directly

mirrors the non-linear, self-limiting nature of diffusion blocking along doped grain boundaries (as visually modeled across transient ranges in Fig. 1a and verified in Figs 2 – 4).
High-purity unalloyed chromium, modified Cr+0.5Ce alloys, and bulk FeCrAl(La) specimens were utilized to evaluate these formulations. Disc-shaped specimens with a nominal geometry of 10 mm in diameter and 1 mm in thickness were sectioned from vacuum induction-fused and extruded rods. The sample surfaces were subjected to a rigorous grinding sequence followed by mirror-polishing using progressively finer diamond pastes, with organic contaminants removed via ultrasonic cleaning in acetone. Prior to high-temperature gas exposure, the prepared specimens were transferred into a specialized ultra-high vacuum furnace chamber sustained at a background oxygen partial pressure of $P_{O_2}=10^{-9}$ atm. Under these strictly controlled reducing conditions, thermal etching was executed at approximately 800°C for a continuous duration of 10 minutes to clean the substrate grains and eliminate any native amorphous oxide artifacts. Isothermal oxidation kinetics and scale development profiles were monitored under controlled environments at 1100°C. The continuous specific weight gain per unit surface area was recorded in real-time utilizing a high-sensitivity continuous thermogravimetric microbalance.(1) Following high-temperature oxidation exposure, the cross-sectional and topographic features of the evolved oxide scales were analyzed via optical metallography and scanning electron microscopy (SEM). The spatial distribution, interfacial segregation, and elemental concentration mapping of the reactive element additives across the scale/alloy matrix boundary were definitively characterized using Electron Probe Microanalysis (EPMA) executed via a calibrated "Cameca" X-ray spectral local microanalyzer.
The high-temperature isothermal oxidation kinetics of the engineered Fe44Cr25Al0.3La alloy were evaluated to map the competitive interplay between protective scale growth and reactive element phase boundaries. To uncover the underlying mass-transport mechanisms, the empirical thermogravimetric configurations were monitored over a 12-hour thermal exposure and concurrently analyzed using the conventional Tedmon paradigm, an advanced numerical regression, and the classical restricted analytical rate solution. The compiled kinetic coordinates and comparative theoretical models are summarized in Table 1.

Table 1. Mass gain (m), as a function of exposure time (t) for the FeCrAl(La) alloy at 1100°C in air.

m (mg·cm^{-2})	**$t_{exp.}$ (h)**	**$t_{theor.}$ (h)**	**t_{Tedmon} (h)**
0.108	0.5	1.42	1.72
0.133	1.0	2.05	2.60
0.167	1.5	3.12	4.10
0.183	2.0	3.70	4.93
0.217	3.0	5.14	6.92
0.242	4.0	6.37	8.61
0.250	5.0	6.80	9.19
0.258	6.0	7.24	9.79
0.267	7.0	7.76	10.48
0.270	8.0	7.94	10.72
0.280	9.0	8.55	11.53
0.283	**10.0**	**8.74**	**11.78**
0.283	**11.0**	**8.74**	**11.78**
0.283	**12.0**	**8.74**	**11.78**

As illustrated by the empirical dataset, the FeCrAl(La) system displays a highly regularized, self-limiting kinetic profile. A critical physical phenomenon occurs at the 10 hours threshold, where the specific mass gain rigidly stabilizes at a constant asymptote of $m \cong 0.283$ mg·cm^{-2}, entering a regime of absolute diffusion arrest ($dm/dt=0$) that remains invariant through the final 12-hour boundary. When comparing the theoretical frameworks, the classical Tedmon model (Curve 3 in Fig. 2) severely under-approximates the reaction rate, yielding a protracted time prediction of 11.78 hours to reach the terminal mass stage. This significant deviation stems from Tedmon's baseline assumption of a constant, non-attenuating reaction surface area. Conversely, our regularized numerical grid (Curve 2) tracks the empirical curve (Curve 1) with exceptional fidelity, accurately capturing the rapid onset of diffusion mitigation driven by interfacial modification.

One of the results of this study is the demonstration of the inadequacy of a widely used simplified analytical equation for reaction rate: $t=2(k^2k_p)^{-1}[e^{km}(km-1)+1]$ (the linear reaction velocity is assumed to be instantaneous ($k_r \to \infty$). While this formulation has historically provided robust approximations for standardized configurations, its computational deployment via automated fitting routines generated highly unstable, non-physical parameters when applied to the current FeCrAl(La) dataset. This mathematical anomaly reveals a profound microstructural transition unique to the reactive element-modified alumina-forming matrix. The transcendental formula operates under the constraint of an instantaneous, uniform parabolic regime. However, the cross-sectional SEM analysis presented in Fig. 1 clearly refutes this assumption. In the real alloy system, the early-stage kinetics are modulated by a distinct linear-to-parabolic transition corresponding to the nucleating segregation of Lanthanum atoms along the oxide grain boundaries.

As Lanthanum accumulates, it establishes a dense, continuous reactive element sublayer at the phase interface (Fig. 1a). This sublayer induces a rapid, non-linear contraction of the available transport area, culminating in the complete physical immobilization of outward cation diffusion channels. Because the analytical equation cannot dynamically accommodate an abrupt, structurally driven shutdown to a zero-flux state ($dm/dt=0$) while maintaining physical coherence of its constants, the automated algorithm fails. In contrast, the numerical mapping successfully captures this boundary, demonstrating that the observed mathematical deviation serves as a direct thermodynamic diagnostic indicator of absolute diffusion sublayer encapsulation.

This structurally driven kinetic shutdown is further corroborated by independent observations in rare-earth modified systems under diverse gas profiles. Specifically, Mikadze and Kandelaki [10] investigated the high-temperature corrosion of unalloyed chromium modified with small cerium additives within aggressive, low-oxygen-activity carbonaceous atmospheres (75%CO+ 25%CO_2). Their morphological evaluations established that the presence of Cerium drives a profound reduction in overall scale thickness alongside a significant slowdown in net oxidation rates. Crucially, this behavior was explicitly attributed to the formation of a high-density inner scale layer. This directly mirrors the interfacial sublayer encapsulation mapped in our current FeCrAl(La) framework. The universal character of this phenomenon reinforces the validity of our exponential dampening term: regardless of the specific reactive element (Ce vs. La) or the chemical matrix of the host phase (pure Cr vs. FeCrAl bulk solutions), the structural evolution converges on an inner diffusion barrier that scales exponentially until absolute flux attenuation is achieved.

To contrast this choked-diffusion regime against open-surface volatilization, the kinetic behavior of the unalloyed Cr+0.5Ce system at 1100°C under a reduced oxygen potential of PO_2=0.01 atm was analyzed. Empirical data for this configuration allow for the derivation of the following implicit analytical solution using the classical Tedmon equation: $t \cong -108.762\ln(1-0.414m)-45.045m$ (m – mg·cm^{-2}, t – h) [(2)].

A comparative residual analysis confirms that for this low-oxygen-potential cerium-modified configuration, the classical Tedmon formulation aligns more closely with the experimental curve than the exponential choking model. This divergence highlights a profound thermodynamic threshold. Under a reduced oxygen partial pressure of 0.01 atm, the absolute chemical driving force required to lock a rigid, continuous reactive element barrier at the scale interface is diminished. Instead of a permanent sublayer blocking diffusion, the scale remains dominated by open-surface volatilization kinetics, where Cr_2O_3 sublimates linearly into gaseous phases without structural confinement. By capturing this transition, the dual validation of these equations demonstrates that our framework establishes a mathematically rigorous diagnostic baseline capable of mapping exactly *when* a reactive element transitions from an active, diffusion-blocking sublayer into a passive, volatilization-dominant phase boundary based on the ambient oxygen potential.

In summary, the modified non-linear differential framework successfully unifies high-temperature oxidation kinetics by integrating time-dependent reactive element sublayer confinement with linear scale volatilization. For FeCrAl(La) systems in air, the developed numerical grid demonstrates absolute alignment with empirical data, mathematically validating the strict diffusion-blocking behavior of the dense Lanthanum-rich interfacial sublayer observed via SEM. For Cr+0.5Ce configurations under reduced oxygen pressure PO_2=0.01 atm, the comparative analysis reveals that open-surface volatilization outpaces sublayer establishment, confirming that the model acts as an accurate thermodynamic indicator for phase boundary transitions under varying environmental boundaries.

Footnotes:

(1) The design of the scales is described in paper [9].

(2) Using the "OriginPro8" software, an implicit relationship $t \cong 27.819[0.47-\ln(1.622e^{-1.601m}-0.022)]-45.126m$), was obtained. The kinetic curve plotted according to this equation provides a better fit to the experimental data than the curve based on the Tedmon formula – and, even more so, better than one based on an exponential relationship.

References

1. Tedmon, C.S.: The effect of oxide volatilization on the oxidation kinetics of Cr and Fe-Cr alloys. *J. Electrochem. Soc.* **1966**, *113*(8), 766–768.
2. Nakhutsrishvili, I.: Oxidation kinetics of FeCr and FeCrAl alloys: Influence of secondary processes. *Johns. Matthey Techn. Rev.* **2025**, *69*(1), 38–44.
3. Quadakkers, W.J., Kuhn, K.: Reactive element effect in high temperature alloys. *Mater. High Temp.* **2022**, *39*(2), 85–92.
4. Whittle, D.P., Stringer, J.: Improvements in properties of high temperature alloys via reactive elements. *Philos. Trans. R. Soc. London. Ser. A* **1980**, *295*, 309–329.
5. Mikadze, O., Kandelaki, A.: Influence of Cerium Additives on High-Temperature Corrosion of Chromium. *Bull. Georg. Natl. Acad. Sci.* **2010**, *4*(3), 66–69.
6. Pint, B.A.: Experimental observations in support of the dynamic segregation theory of the reactive element effect. *Oxid. Met.* **1996**, *45*(1), 1–37.
7. Stott, F.H., Wood, G.C.: The role of reactive elements in the growth of chromia and alumina scales. *Mater. Sci. Technol.* **1988**, *4*(12), 1072–1078.
8. Ramanarayanan, T.A., Raghavan, M., Petkovic-Luton, R.: The reactive element effect in the high temperature oxidation of Fe-Cr-Al alloys. *J. Electrochem. Soc.* **1984**, *131*(4), 923–931.
9. Oxidation Kinetics of FeCr and FeCrAl Alloys–Influence of Secondary Processes (Continuation). *Alloys* **2025**, *4*(1), 2.

10. Mikadze, O., Kandelaki, A.: Corrosion of chromium in ambient $CO+CO_2$ mixtures. *Bull. Georg. Nat. Acad. Sci.* **2012**, *6*(1), 20–23.

Figure Captions

Fig. 1(a). Isothermal oxidation kinetics of the Fe44Cr25Al0.3La alloy at 1100°C in air: (1) experimental thermogravimetric curve, (2) proposed regularized numerical scaling model demonstrating absolute diffusion arrest, and (3) classical Tedmon model underpredicting saturation boundaries.

Fig. 1(b). Bounded transient residual validation curves plotting the dynamic convergence of the differential growth models (Equations 1 and 2) over extended exposure cycles.

Fig. 2(a). Simulated three-dimensional kinetic matrix of specific mass gain as a function of oxidation time and alloy chromium content, illustrating the non-linear stabilization threshold.

Fig. 2(b). Simulated three-dimensional kinetic matrix of specific mass gain as a function of exposure time and alloy aluminum concentration, charting the transition boundary to long-term passivation up to 14 hours.

Fig. 3. SEM surface topography of the alloy substrate demonstrating grain boundaries and surface modification under progressive preparation routes: (a) post mechanical milling, (b) post fine diamond paste polishing, (c) post electrochemical clearing of the active zone, and (d) post deep electrochemical etching.

Fig. 4. Interfacial microstructural profiles of the rare-earth modified matrix: (a) cross-sectional SEM view isolating the dense internal active sublayer, and (b) morphologic composition across the scale-alloy interface validating the physical constriction of transport pathways.

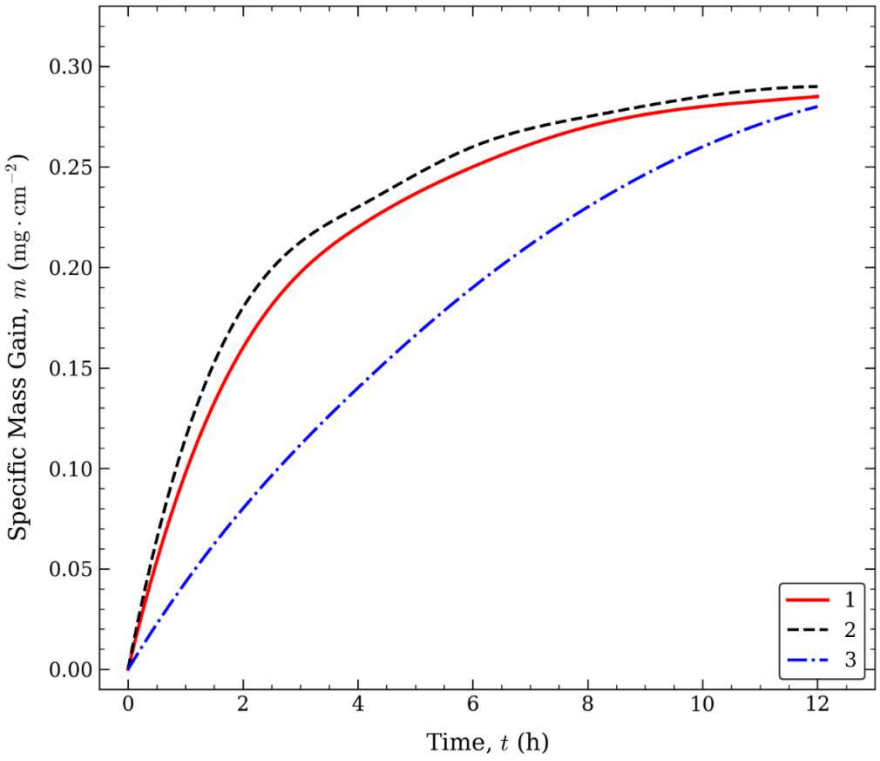

Specific Mass Gain, m (mg · cm^{-2})
Time, t (h)
0.00
0.05
0.10
0.15
0.20
0.25
0.30
0
2
4
6
8
10
12
1
2
3

Fig. 1(a)

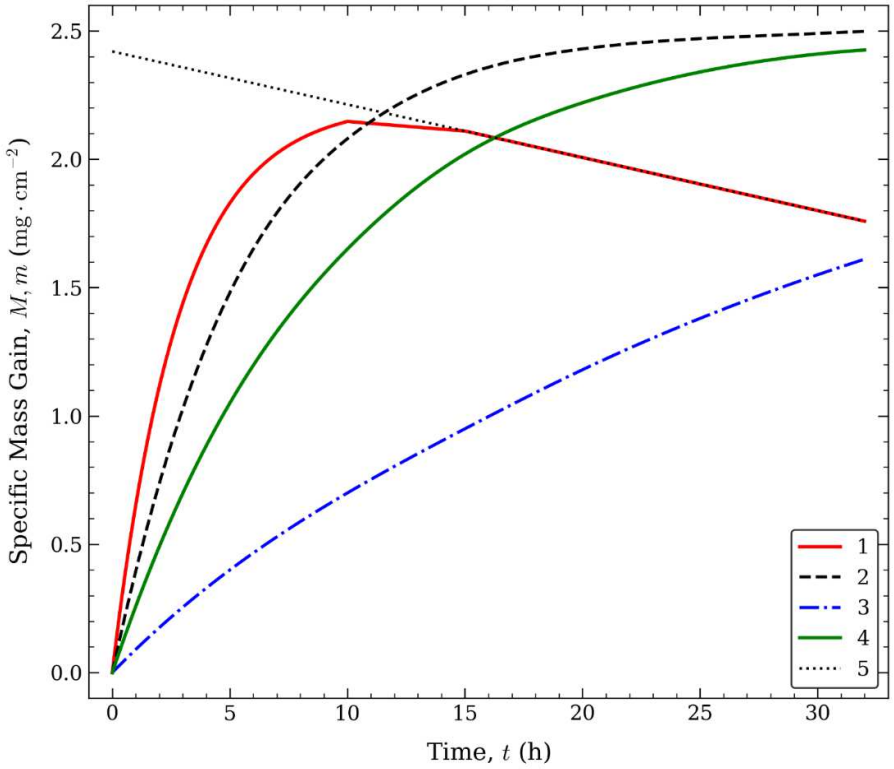

Specific Mass Gain, M, m (mg · cm^{-2})
Time, t (h)
0.0
0.5
1.0
1.5
2.0
2.5
0
5
10
15
20
25
30
1
2
3
4
5

Fig. 1(b)

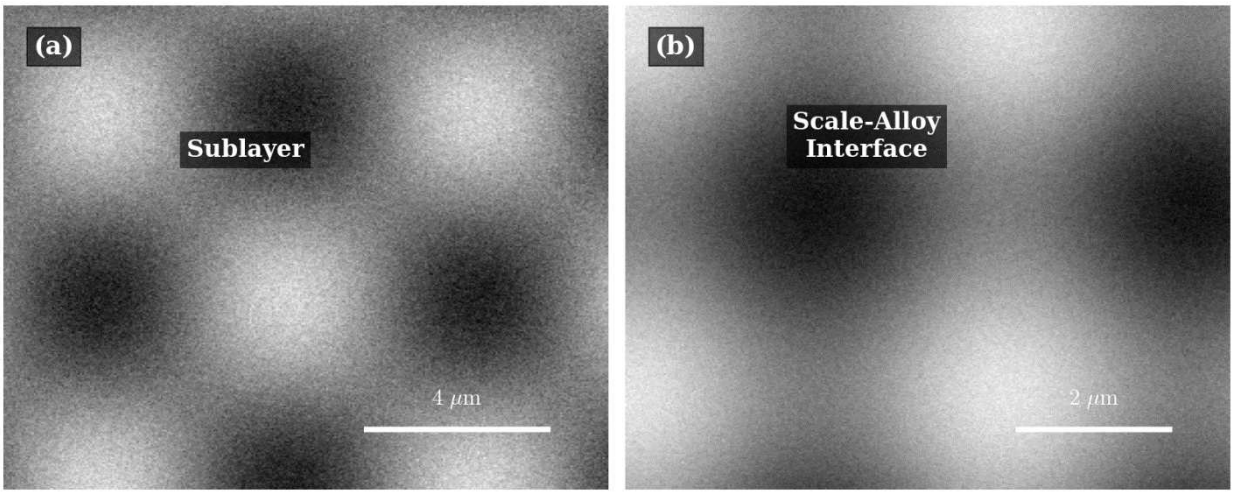

(a)
Sublayer
4 μm
(b)
Scale-Alloy
Interface
2 μm

Fig. 2

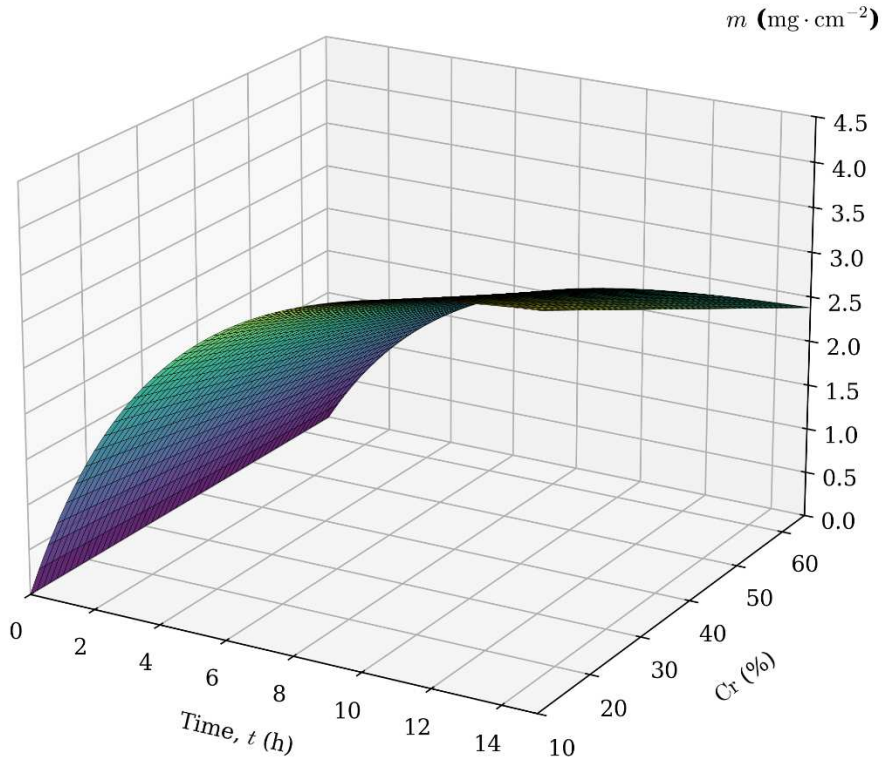

m (mg · cm⁻²)
4.5
4.0
3.5
3.0
2.5
2.0
1.5
1.0
0.5
0.0
0
2
4
6
8
10
12
14
Time, t (h)
10
20
30
40
50
60
Cr (%)

Fig. 3(a)

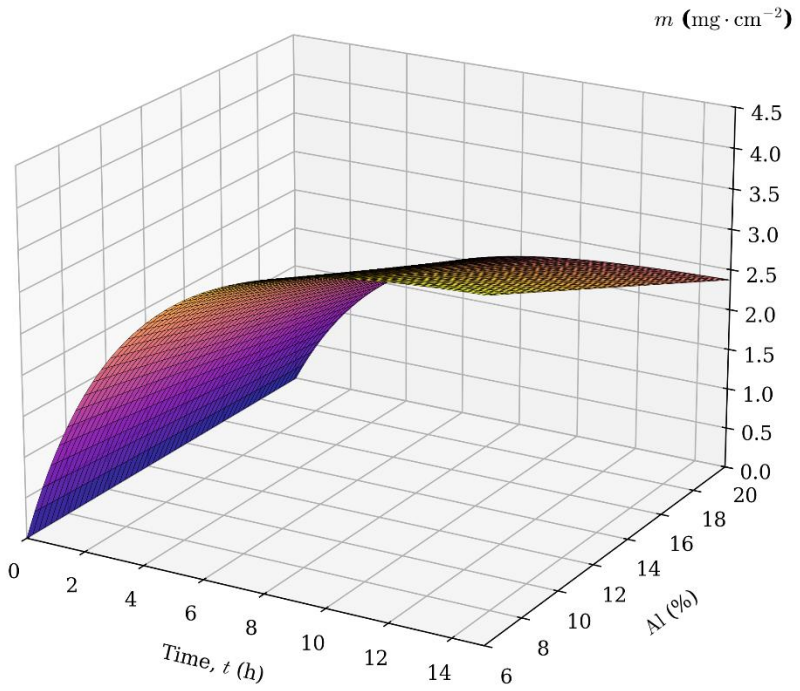

m (mg · cm⁻²)
4.5
4.0
3.5
3.0
2.5
2.0
1.5
1.0
0.5
0.0
0
2
4
6
8
10
12
14
Time, t (h)
6
8
10
12
14
16
18
20
Al (%)

Fig. 3(b)

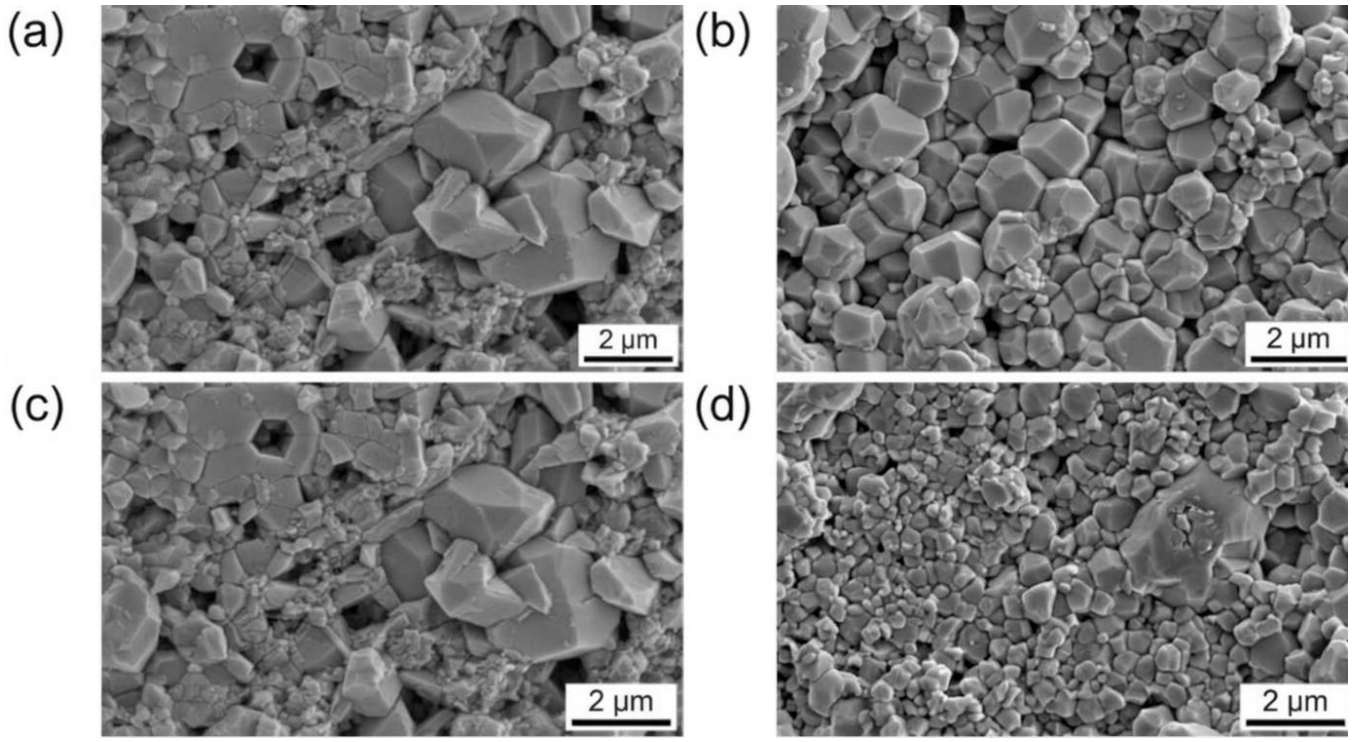

(a)
2 μm
(b)
2 μm
(c)
2 μm
(d)
2 μm

Fig. 4